

Effective interactions in colloid - semipermeable membrane systems

Paweł Bryk

*Department for the Modeling of Physico-Chemical Processes,
Maria Curie-Skłodowska University, 20-031 Lublin, Poland**

(Dated: November 20, 2018)

We investigate effective interactions between a colloidal particle, immersed in a binary mixture of smaller spheres, and a semipermeable membrane. The colloid is modeled as a big hard sphere and the membrane is represented as an infinitely thin surface which is fully permeable to one of the smaller spheres and impermeable to the other one. Within the framework of the density functional theory we evaluate the depletion potentials, and we consider two different approximate theories - the simple Asakura-Oosawa approximation and the accurate White-Bear version of the fundamental measure theory. The effective potentials are compared with the corresponding potentials for a hard, nonpermeable wall. Using statistical-mechanical sum rules we argue that the contact value of the depletion potential between a colloid and a semipermeable membrane is smaller in magnitude than the potential between a colloid and a hard wall. Explicit calculations confirm that the colloid-semipermeable membrane effective interactions are generally weaker than these near a hard nonpermeable wall. This effect is more pronounced for smaller osmotic pressures. The depletion potential for a colloidal particle inside a semipermeable vesicle is stronger than the potential for the colloidal particle located outside of a vesicle. The asymptotic decay of the depletion potential for the semipermeable membrane is similar to that for the nonpermeable wall and reflects the asymptotics of the total correlation function of the corresponding binary mixture of smaller spheres. Our results demonstrate that the ability of the membrane to change its shape constitutes an important factor in determining the effective interactions between the semipermeable membrane and the colloidal macroparticle.

I. INTRODUCTION

Depletion interactions play an important role in determining the stability of colloidal systems^{1,2}. They arise in asymmetric mixtures³ due to a tendency to maximize volume available to centers of smaller species. In suitably prepared colloidal suspensions, such that only bare hard-core interactions are left, these effective interactions are attractive at small distances and can exhibit a potential barrier and an oscillatory tail for large separations^{4,5}. Depletion forces also arise if a big colloidal particle suspended in a sea of small particles approaches a fixed object such as a planar wall.

The first theoretical approach to calculate the effective interactions was performed by Asakura and Oosawa⁶, and later, by Vrij⁷. The resulting effective potential is attractive at small distances and proportional to the packing fraction of the depleting agent. More recent approaches include various integral equation^{8,9,10,11} and density functional theories^{12,13,14}. Several experimental techniques have been developed to investigate depletion interactions. Total internal reflection microscopy has been used to investigate depletion potentials between a wall and a sphere immersed in a sea of spherical polymers¹⁵ and rod-like particles^{16,17}. Video-microscopy has been used to measure the depletion potential between two big particles¹⁸, the potential of a big colloid near an edge of a terrace²⁰ and the potential of a big colloid sphere inside a vesicle²¹. In the latter experiment it has been observed that the big particle is attracted to regions of high local curvature. This attraction may in turn induce transformation of the shape of a membrane. Thus the depletion interactions between a colloidal particle and

a membrane may be helpful in a better understanding of many biological processes.

Theoretical attempts to describe the colloid-vesicle experiment were initiated by Roth *et al.*²² who used density functional theory (DFT) to study depletion forces between a big hard sphere, immersed in a sea of smaller spheres, and a hard, nonpermeable spherical wall. These authors also presented a simple framework for tackling cavities of a general shape. A more refined approach was presented very recently^{23,24}. Bickel investigated depletion interactions near soft, fluctuating surfaces and showed a mechanism for an encapsulation of the colloidal macroparticle²⁵. In all these studies the membrane itself is assumed to be nonpermeable. However, an inherent attribute of a semipermeable membrane system is the presence of a fluid on both membrane sides. The difference in composition of the fluid on both sides, which appears due to the selective permeability of a membrane, gives rise to the osmotic pressure.

Several microscopic models of semipermeable membrane systems have been proposed in the literature²⁶. The simplest model is the so-called ideal membrane - an infinitely thin surface which is fully permeable to some of the species and nonpermeable to others. The fluid structure near such a membrane can be ascertained by means of first^{27,28} and second order²⁹ integral equation theories or DFT³⁰. A somewhat more sophisticated model accounts for finite thickness by treating the membrane as a potential barrier of a finite height and width^{31,32,33}. Finally, in some studies the discrete structure of a membrane was also taken into account by considering membranes built of particles arranged either randomly³⁸ or in a regular manner^{34,35,36,37}.

In the present paper we investigate the effective interactions between a semipermeable membrane and a big colloidal macroparticle. We use the reliable DFT approach that was used previously to study depletion potentials near impenetrable surfaces and inside hard-sphere cavities. This enables us to make a direct comparison and elucidate the effect of the semipermeability on the effective interactions. The paper is arranged as follows: in Section II we consider sum rules for semipermeable membranes. Section III outlines the theories applied in the present paper. Section IV presents results and we conclude in Section V.

II. SUM RULES FOR SEMIPERMEABLE MEMBRANES

Consider two component mixture of species A and B and diameters σ_A and σ_B , respectively. The membrane is fully permeable to the component A but is nonpermeable to the component B . In the course of the derivation we consider the ideal membrane of the spherical shape - a simple model for a semipermeable vesicle. The sum rule for semipermeable planar membrane is then obtained by taking the limit $R_M \rightarrow \infty$. The membrane is modeled by imposing an external potential of the form

$$V_A^{ext}(r) \equiv 0; \quad V_B^{ext}(r) = \begin{cases} 0, & r > R_M \\ \infty, & r < R_M. \end{cases} \quad (1)$$

In Eq. (1) $R_M = R_M^{(b)} + \sigma_B/2$, and $R_M^{(b)}$ denotes the actual membrane radius (the dashed circle in Fig. 1). R_M stands for the radius at which the profile of the nonpermeable species makes a jump (the solid circle in Fig. 1). The membrane separates the two parts of the system: part II with a two-component fluid and part I, available only to the permeable component. The bulk densities in part II, $\rho_A^{(II)}$ and $\rho_B^{(II)}$, are the input to the calculations. The system is in the thermodynamical but not mechanical equilibrium. The pressure p is different in the two parts of the system and we define the osmotic pressure as

$$\Pi = p^{(II)}(\rho_A^{(II)}, \rho_B^{(II)}) - p^{(I)}(\rho_A^{(I)}). \quad (2)$$

The bulk density in the one-component part of the system, $\rho_A^{(I)}$, is obtained by imposing the equality of the chemical potentials of the permeable component in both parts of the system

$$\mu_A^{(II)}(\rho_A^{(II)}, \rho_B^{(II)}) = \mu_A^{(I)}(\rho_A^{(I)}). \quad (3)$$

It is clear that the osmotic pressure defined by Eqs. (2) and (3) depends only on the equation of state of the system and is independent of the shape of the membrane.

We decompose the grand canonical potential of the system Ω into a reference, bulk part $\Omega^{bulk} = -p^{(II)}V^{(II)} - p^{(I)}V^{(I)}$, where $V^{(I)}$ and $V^{(II)}$ are the volumes of parts I and II, respectively, and to an excess part Ω^{ex} : $\Omega =$

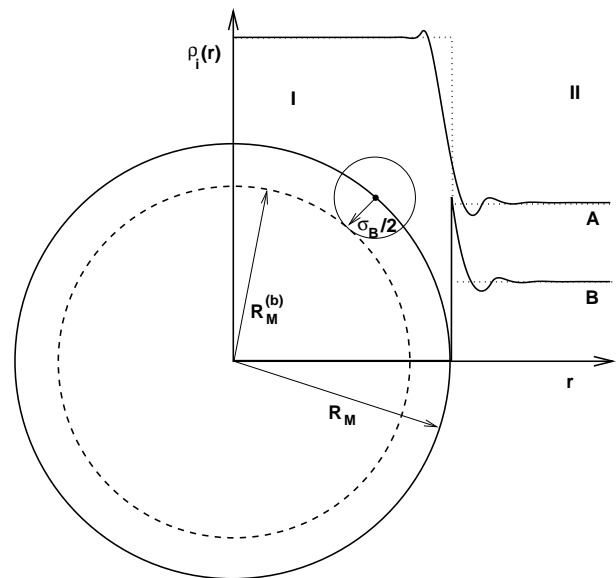


FIG. 1: Schematic plot of a semipermeable vesicle system.

$\Omega^{bulk} + \Omega^{ex}$. We choose R_M and the corresponding spherical surface of the area $4\pi R_M^2$ as the dividing interface. This implies that the volumes of both parts are: $V^{(I)} = 4/3\pi R_M^3$, and $V^{(II)} = 4/3\pi(\bar{R}^3 - R_M^3)$, whereas the densities in the reference system are

$$\begin{aligned} \rho_A^{bulk} &= \rho_A^{(I)}\Theta(R_M - r) + \rho_A^{(II)}\Theta(r - R_M) \\ \rho_B^{bulk} &= \rho_B^{(II)}\Theta(r - R_M), \end{aligned} \quad (4)$$

where θ is the Heaviside unit-step function (cf. dotted lines in Fig. 1). \bar{R} is a macroscopically large radius considered in the thermodynamical limit. Denoting the excess grand potential per unit area as the surface tension γ , we have

$$\Omega = \gamma(R_M)4\pi R_M^2 - p^{(II)}V^{(II)}(R_M) - p^{(I)}V^{(I)}(R_M). \quad (5)$$

We derive the sum rules for semipermeable membranes by expressing the grand potential as a functional of the local densities

$$\Omega[\rho_A, \rho_B] = F[\rho_A, \rho_B] + \sum_{i=A,B} \int d^3r \rho_i(\mathbf{r})(V_i^{ext}(\mathbf{r}) - \mu_i), \quad (6)$$

where F is the Helmholtz free energy functional that will be defined later. The only explicit dependence of Ω on R_M is contained in the second term in the right-hand side of Eq. (6). At thermodynamical equilibrium the grand potential satisfies the Euler-Lagrange equation

$$\frac{\delta\Omega[\rho_A, \rho_B]}{\delta\rho_A(\mathbf{r})} = \frac{\delta\Omega[\rho_A, \rho_B]}{\delta\rho_B(\mathbf{r})} = 0. \quad (7)$$

The sum rules are obtained by taking the derivative of the grand potential Eq. (6) with respect to R_M , at

constant chemical potentials μ_i and temperature T

$$\left(\frac{\partial\Omega}{\partial R_M}\right)_{\mu_i,T} = \sum_{i=A,B} \int d^3r \frac{\delta\Omega[\rho_A,\rho_B]}{\delta\rho_i(\mathbf{r})} \frac{\partial\rho_i(\mathbf{r})}{\partial R_M} + \sum_{i=A,B} \int d^3r \rho_i(\mathbf{r}) \frac{\partial V_i^{ext}(\mathbf{r})}{\partial R_M}. \quad (8)$$

By virtue of Eq. (7) the first sum on the right-hand side of Eq. (8) vanishes whereas the second term yields $\beta^{-1}4\pi R_M^2 \rho_B(R_M^+)$, where $\rho_B(R_M^+)$ is the contact density of the nonpermeable component of a fluid mixture at the ideal semipermeable vesicle. Thus the sum rule reads

$$\beta \left(\frac{\partial\Omega}{\partial R_M}\right)_{\mu,T} = 4\pi R_M^2 \rho(R_M^+), \quad (9)$$

and is satisfied by all density functionals within weighted-density approximation^{39,40,41}.

Taking the derivative of Eq. (5) with respect to R_M and inserting to Eq. (9) the sum rule can be expressed as

$$\rho_B(R_M^+) = \beta\Pi + \frac{2\beta\gamma(R_M)}{R_M} + \beta \left(\frac{\partial\gamma(R_M)}{\partial R_M}\right)_{\mu,T}. \quad (10)$$

In the limit $R_M \rightarrow \infty$ only the first term of Eq. (10) survives and we recover the planar result^{28,42,43,44} that the contact value of the density profile of the nonpermeable species at the planar semipermeable membrane is equal to the osmotic pressure. Since Π is always lower than $p^{(II)}$ we conclude that for the same fluid the contact value at the membrane is lower than the sum of the contact values at a nonpermeable hard wall⁴⁵. One can also consider the case in which the two component mixture is inside the vesicle and the permeable component is present outside the vesicle, i.e. the ‘‘reverse’’ of the situation plotted in Fig. 1. In this case the contact value of the nonpermeable component will be higher than that at the planar membrane.

III. THEORY FOR DEPLETION POTENTIALS

We consider a single big colloidal hard-sphere of diameter σ_C immersed in a two-component mixture of smaller hard-sphere of diameters σ_A and σ_B , respectively. The system is in contact with an ideal semipermeable membrane which is permeable to the A component but nonpermeable to the B component, as well as to the big sphere C . We also assume that $\sigma_A < \sigma_B < \sigma_C$. The goal is to evaluate the effective depletion potential W between the big colloidal hard-sphere and the semipermeable membrane. In our study we use a versatile approach proposed in Refs.^{13,14}. According to this theory the depletion potential is evaluated on the basis of the density profiles of the small spheres undisturbed by the presence of the big sphere. In the dilute limit of the big spheres ($\rho_C \rightarrow 0$ or, equivalently, $\mu_C \rightarrow -\infty$) the depletion potential W at a point \mathbf{r} can be expressed in terms of

the difference between the one-particle direct correlation function $c_C^{(1)}$ in the bulk ($\mathbf{r} \rightarrow \infty$) and at \mathbf{r}

$$\beta W(\mathbf{r}) = \lim_{\rho_C \rightarrow 0} \left(c_C^{(1)}(\mathbf{r} \rightarrow \infty) - c_C^{(1)}(\mathbf{r}) \right). \quad (11)$$

A convenient route for the evaluation of $c_C^{(1)}(\mathbf{r})$ is provided by density functional theory⁴⁶. The focal point in this approach is the excess (over the ideal gas) free energy, $F_{ex} = F - \sum_i \int d^3\mathbf{r} \{\rho_i(\mathbf{r}) \ln(\rho_i(\mathbf{r})) - 1\}$. The one-particle direct correlation function is then directly accessible via

$$c_C^{(1)}(\mathbf{r}) = -\beta \frac{\delta F_{ex}}{\delta \rho_C(\mathbf{r})}. \quad (12)$$

For mixtures of hard-spheres the exact excess free energy formula is not known and some approximations are required. In this work we consider two approximate functionals. The first one is the low density limit functional

$$\beta F_{ex} = -\frac{1}{2} \sum_{i,j} \int d^3r \int d^3r' \rho_i(\mathbf{r}) \rho_j(\mathbf{r}') f_{ij}(\mathbf{r}-\mathbf{r}'), \quad (13)$$

where f_{ij} is the Mayer bond between a particle of species i and a particle of species j . In the low density limit the density profiles $\rho_A(\mathbf{r})$ and $\rho_B(\mathbf{r})$ tend to ρ_A^{bulk} and ρ_B^{bulk} , respectively. Then from Eqs. (11)-(13) we obtain the Asakura-Oosawa approximation for the depletion potential

$$\beta W^{AO}(\mathbf{r}) = - \sum_{i=A,B} \int d^3r' (\rho_i^{bulk} - \rho_i^{(II)}) f_{iC}(\mathbf{r}-\mathbf{r}'), \quad (14)$$

where $f_{iC}(\mathbf{r}-\mathbf{r}') = -\Theta((\sigma_i + \sigma_C)/2 - |\mathbf{r}-\mathbf{r}'|)$. Equation (14) implies that W^{AO} is identically zero for distances larger than σ_B from the membrane.

The second approximate functional considered in this work is Rosenfeld’s Fundamental Measure Theory⁴⁷ (FMT). Within this approach the excess free energy of an N component hard-sphere mixture is given by

$$\beta F_{ex} = \int d^3r \Phi(\{n_\alpha\}), \quad (15)$$

where n_α denote weighted densities

$$n_\alpha(\mathbf{r}) = \sum_{j=1}^N \int d^3r' \rho_j(\mathbf{r}') w_\alpha^{(j)}(\mathbf{r}-\mathbf{r}'). \quad (16)$$

The weight functions $w_\alpha^{(j)}$ depend of geometrical properties of individual species, see earlier papers for explicit formulas^{47,48}.

From a number of prescriptions for the excess free energy density Φ , for the given problem we have chosen the elegant and inspiring White-Bear (WB) formula^{49,50}

$$\Phi(\{n_\alpha\}) = -n_0 \ln(1 - n_3) + \frac{n_1 n_2 - \mathbf{n}_{V1} \cdot \mathbf{n}_{V2}}{1 - n_3} + (n_2^3 - 3n_2 \mathbf{n}_{V2} \cdot \mathbf{n}_{V2}) \frac{n_3 + (1 - n_3)^2 \ln(1 - n_3)}{36\pi(n_3)^2(1 - n_3)^2} \quad (17)$$

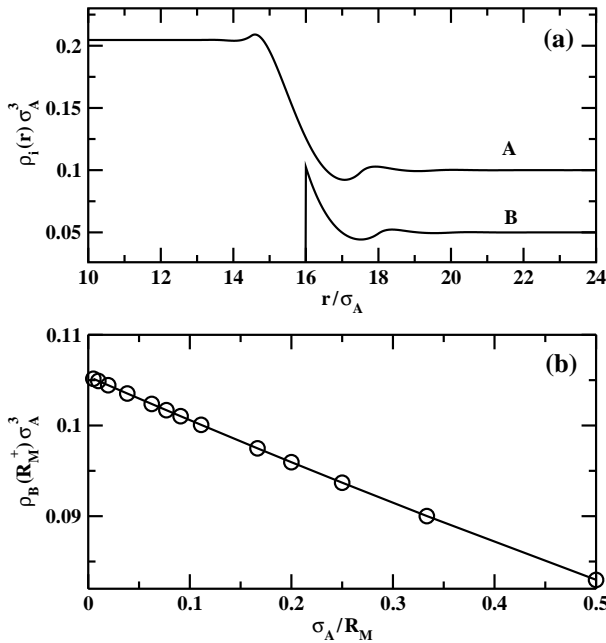


FIG. 2: (a) Density profiles of a hard-sphere mixture near a semipermeable vesicle. The bulk densities are $\rho_A^{(II)}\sigma_A^3 = 0.1$ and $\rho_B^{(II)}\sigma_A^3 = 0.05$. (b) The contact value of the density profile of the nonpermeable component (solid line) and the right-hand side of the sum rule, Eq.10 (circles) plotted as a function of the inverse membrane radius, R_M .

As explained in^{13,14} FMT provides a very nice method of calculating the depletion potentials. In the present case of a ternary hard-sphere mixture the dilute limit of species C can be obtained by considering the set of restricted weighted densities

$$n_\alpha^{dil}(\mathbf{r}) = \sum_{j=A,B} \int d^3r' \rho_j(\mathbf{r}') w_\alpha^{(j)}(\mathbf{r} - \mathbf{r}'). \quad (18)$$

The depletion potential is then obtained from

$$\beta W^{WB}(\mathbf{r}) = \sum_\alpha \int d^3r' \Psi_\alpha(\mathbf{r}'; \{n_\alpha^{dil}\}) w_\alpha^{(C)}(\mathbf{r} - \mathbf{r}'), \quad (19)$$

where

$$\Psi_\alpha(\mathbf{r}'; \{n_\alpha^{dil}\}) = \beta \left(\frac{\partial \Phi(\{n_\alpha^{dil}\})}{\partial n_\alpha^{dil}} \right)_{\mathbf{r}'} - \beta \left(\frac{\partial \Phi(\{n_\alpha^{dil}\})}{\partial n_\alpha^{dil}} \right)_{\infty}. \quad (20)$$

The computational strategy consists of two stages. First the profiles for the binary $A+B$ mixture are evaluated by minimizing the White-Bear version of the fundamental measure functional. The resulting set of restricted weighted densities is then used as an input to a separate program, in which the depletion potentials are computed by applying Eqs. (19)-(20). The strategy outlined above offers an important advantage, because the computational problem is effectively reduced from three-component to two-component mixture. This method is especially appreciated when the density profile is a function of more than one scalar⁵¹.

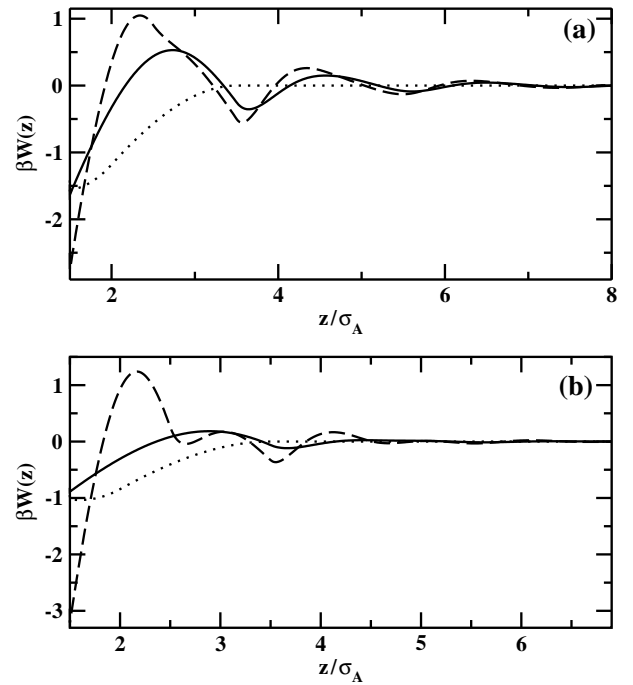


FIG. 3: Depletion potentials for a single big hard sphere C immersed in a mixture of hard spheres $A+B$ of diameters $\sigma_B = 2\sigma_A$. The diameter of the big hard sphere $\sigma_C = 3\sigma_A$. The solid lines denote depletion potentials between a big hard sphere and a semipermeable planar membrane evaluated from the WB theory. The dashed lines denote depletion potentials for the same mixture but at a hard nonpenetrable wall evaluated from the WB theory. The dotted lines denote depletion potentials at a semipermeable planar membrane evaluated using AO approximation. Packing fractions are $\eta_A = 0.05$, $\eta_B = 0.35$ in (a) and $\eta_A = 0.15$, $\eta_B = 0.25$ in (b).

IV. RESULTS AND DISCUSSION

A. Depletion Potentials

Typical density profiles resulting from the WB theory are displayed in the upper panel of Fig. 2. The profiles were evaluated for a binary hard sphere mixture of sizes $\sigma_B = 2\sigma_A$ near a semipermeable vesicle of the size $R_M = 16\sigma_A$. The bulk densities are $\rho_A^{(II)}\sigma_A^3 = 0.1$ and $\rho_B^{(II)}\sigma_A^3 = 0.05$. The osmotic pressure $\beta\Pi\sigma_A^3 = 0.105\ 391\ 59$. The contact value of the density profile $\rho_B(R_M^+) = 0.102\ 373\ 22$ whereas the right-hand-side of Eq. (10) is $0.102\ 373\ 78$. Similar level of agreement was found for other radii and this confirms high accuracy of the numerical results. The plot of the contact value as a function of the inverse membrane radius evaluated for these bulk densities is shown in the lower panel of Fig. 2. In the planar membrane limit, $\sigma_A/R_M = 0$ the contact value tends to the osmotic pressure.

We turn now to the depletion potentials. In order to restrict a rather large parameter space we consider the case of the fixed diameters of smaller spheres $\sigma_B = 2\sigma_A$.

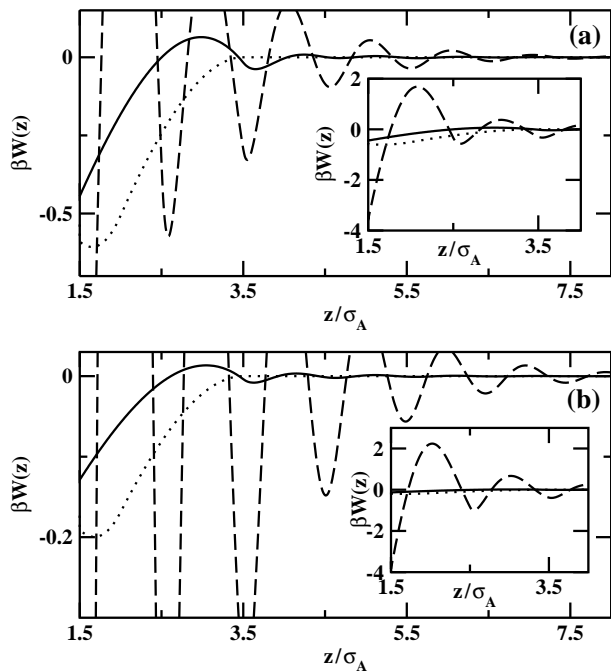


FIG. 4: The same as in Fig. 3 but now for packing fractions $\eta_A = 0.25$, $\eta_B = 0.15$ in (a) and $\eta_A = 0.35$, $\eta_B = 0.05$ in (b). The insets show the zoom-out of the main figures.

Moreover, we consider the case of a constant total packing fraction $\eta = \sum_{i=A,B} \eta_i = \sum_{i=A,B} (\pi/6) \rho_i^{(II)} \sigma_i^3 = 0.4$ and the case of a fixed $\eta_B = 0.15$. By varying packing fraction of the components we have a possibility to investigate fairly dense systems but with different osmotic pressures. Thus we hope to draw rather general conclusions.

Figures 3 and 4 show the depletion potentials between a big colloidal particle of the size $\sigma_C = 3\sigma_A$ and a planar semipermeable membrane, plotted as a function of the distance to the membrane surface z . The potentials were evaluated for the constant total packing fraction $\eta = 0.4$.

The solid lines are the results of the WB theory whereas the dotted lines denote the results of the AO approximation. The dashed lines denote W^{WB} but for the planar, nonpenetrable wall. We observe that the differences between the colloid-wall and the colloid-membrane potentials are rather significant. In all cases the effect of the membrane permeability is to decrease the effective interactions, relative to the hard wall. The oscillations are less pronounced and the contact values of the depletions potentials are smaller in magnitude. These trends are already well visible for small packing fractions of the smaller spheres (cf. Fig. 3a, $\eta_A = 0.05$, $\eta_B = 0.35$) and increase with η_A (cf. Fig. 3b, $\eta_A = 0.15$, $\eta_B = 0.25$). For high packing fractions of the smaller spheres and low η_B , (see Fig. 4) the difference between the corresponding potentials is rather dramatic. The contact value of βW for the membrane is less than -0.5 whereas for the hard wall this value is around -4 (see the insets to Fig. 4). Note

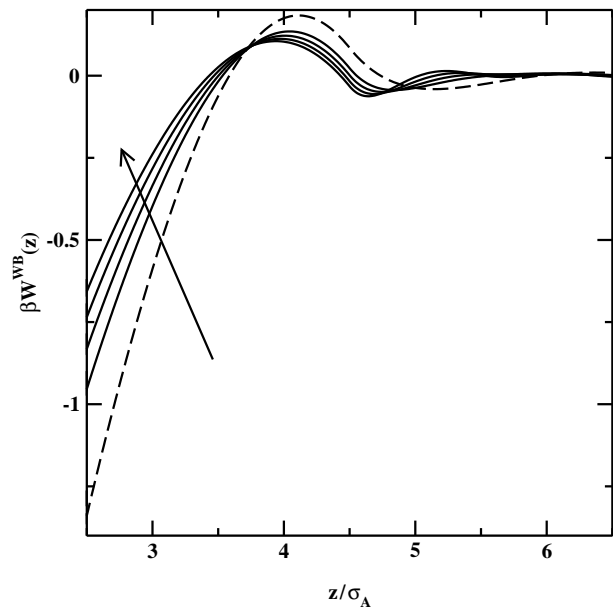


FIG. 5: Depletion potentials for a single big colloidal sphere of diameter $\sigma_C = 5\sigma_A$ near a semipermeable planar membrane. The packing fraction of the nonpermeable component $\eta_B = 0.15$, and $\sigma_B = 2\sigma_A$. The solid lines denote the potentials for the packing fractions of the permeable component $\eta_A = 0.10, 0.15, 0.20$, and 0.25 . The arrow indicates the increase of η_A . The dashed line indicates the result for $\eta_A = 0$.

also that the oscillations, and in particular the first maximum, are significantly smaller for the membrane than for the wall.

That the depletion potential near a semipermeable membrane is weaker than the potential near a nonpermeable wall can be anticipated already from Eq. (10). For the one-component hard sphere system the contact value of the depletion potential, as predicted by the accurate parameterization¹⁴, is linear in the packing fraction of the small spheres. The packing fraction of the small spheres itself is related to the contact value of the profile near the wall, thus the higher the pressure and the contact value of the density profile, the stronger the depletion potential. While for mixtures such parameterization is unknown it is reasonable to assume a similar behavior. Since the contact value near the membrane is always lower, the depletion potential is expected to be weaker and this is confirmed by the explicit calculations.

It is interesting to note that the simple Asakura-Oosawa approximation (dotted lines in Figs. 3 and 4) performs relatively well when compared with the WB theory. It is clear that the AO approximation cannot account for the oscillatory part of the depletion potential but the contact value resulting from this approach does not differ too much from the accurate WB theory.

Figure 5 shows the depletion potentials between a single big colloidal particle of the size $\sigma_C = 5\sigma_A$ and a semipermeable planar membrane, evaluated for a constant packing fraction of the nonpermeable component

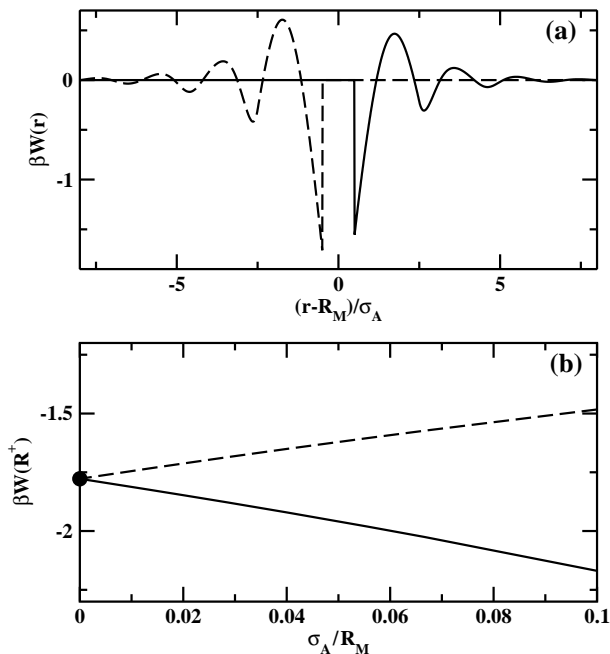


FIG. 6: (a) Depletion potentials between a single big colloidal sphere of diameter $\sigma_C = 3\sigma_A$ and a semipermeable vesicle of the radius $R_M = 20\sigma_A$ plotted as a function of the relative distance to the vesicle $(r - R_M)/\sigma_A$. The solid line denotes the potential for the system in which the two component part of the system is located outside of the vesicle whereas the dashed line denotes the potential the system in which the two component part of the system is located inside the vesicle. The packing fractions $\eta_A = 0.05$ and $\eta_B = 0.35$. (b) Contact value of the depletion potential between a single big colloidal sphere of diameter $\sigma_C = 5\sigma_A$ and a semipermeable vesicle plotted as a function of the vesicle curvature. The solid line denotes the potential for the system in which the two component part of the system is located outside of the vesicle whereas the dashed line denotes the potential the system in which the two component part of the system is located inside the vesicle. The packing fractions $\eta_A = 0.30$ and $\eta_B = 0.10$. Black dot indicates the planar result limit.

$\eta_B = 0.15$ and for different packing fractions of the permeable component $\eta_A = 0.10, 0.15, 0.20$, and 0.25 . The direction of the increase of η_A is indicated by the arrow and it is also the direction of decreasing osmotic pressure. We observe that for constant η_B the effective interactions get stronger with an osmotic pressure increase (the same trend is observed in Figs. 3-4). For reference we also show the potential for $\eta_A = 0$ (dashed line) and it is clearly the strongest potential for this η_B .

Finally in Fig. 6 we show the influence of the curvature of the membrane on the depletion potentials. We consider the depletion potential near a convex and a concave semipermeable membrane. This corresponds to the cases where the two component part of the system is located outside of, and inside the vesicle, respectively. Similar to the hard wall case²² we find that the depletion potential inside the vesicle is stronger, whereas the

potential outside of the vesicle weaker, than the corresponding potential at the planar membrane (cf. Fig. 6a). However, this effect is moderated in comparison to the hard wall case because, in general, the depletion potentials near semipermeable membranes are weaker. Figure Fig. 6b shows the contact value of the depletion potential at a semipermeable membrane plotted as a function of the inverse vesicle radius. We find that, although the convergence to the planar membrane result (marked by the black dot) is rather slow, one has to go to rather small radii in order to noticeably increase/decrease the contact value of the depletion potential.

B. Asymptotic behavior

The behavior of the depletion potential at large separations can be ascertained by using the general theory of asymptotics of pair correlations functions^{52,53}. It was demonstrated that the decay of many structural properties of inhomogeneous fluids such as density profile, solvation force and depletion potential¹⁴ should be the same as the asymptotics of the bulk pair correlation functions h_{ij} . Recently Grodon *et al.*^{54,55} presented a detailed investigation of the asymptotic decay of pair correlation functions in binary hard-sphere mixtures. The main finding is that for sufficiently asymmetric mixtures there is a structural crossover line in the (η_A, η_B) plane which separates two distinct regimes of the asymptotic decay. Below we recall main predictions of the general theory of asymptotics of pair correlations functions for mixtures.

The Fourier transforms of the total correlation functions for a binary mixture of A and B species can be written as

$$\hat{h}_{ij}(k) = \frac{\hat{N}_{ij}(k)}{\hat{D}(k)} \quad i, j = A, B. \quad (21)$$

While the nominators $\hat{N}_{ij}(k)$ in Eq. (21) are different for different pairs ij , all three total correlation functions have the same denominator $\hat{D}(k)$

$$\hat{D}(k) = [1 - \rho_A \hat{c}_{AA}^{(2)}(k)][1 - \rho_B \hat{c}_{BB}^{(2)}(k)] - \rho_A \rho_B \hat{c}_{AB}^{(2)}(k)^2. \quad (22)$$

In the above $\hat{c}_{ij}^{(2)}(k)$ is the Fourier transform of the (two-particle) direct correlation function. The inverse Fourier transform of Eq. (22) is formally obtained via the residue theorem. While in general an infinite number of residues and the corresponding poles contributes to $h_{ij}(r)$, the asymptotic decay is governed by the leading order pole $p^{(LO)} = \pm a_1 + ia_0$, that is by the pole with the smallest imaginary part. Close to a crossover point two poles $p^{(1)} = a_1 + ia_0$ and $p^{(2)} = \tilde{a}_1 + i\tilde{a}_0$ have similar imaginary parts and both contribute to the decay. Provided that the Fourier transforms of $c_{ij}(r)$ are known analytically, the poles can be conveniently determined by finding complex solutions to the equation $\hat{D}(k) = 0$. In the present case of the binary hard-sphere mixture the direct correlation

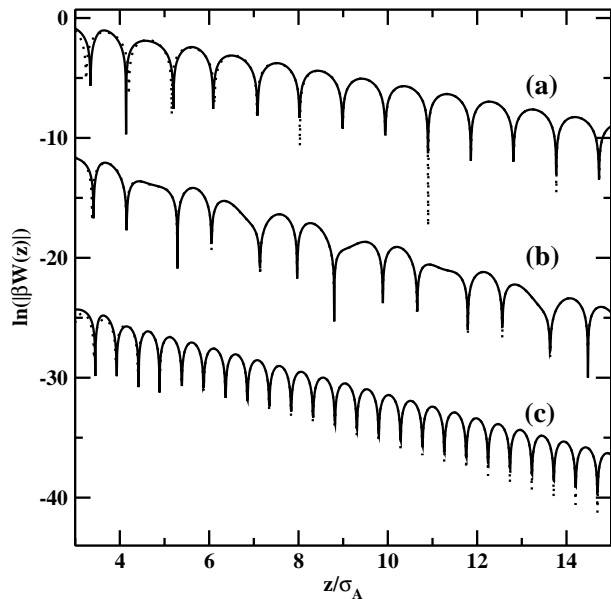


FIG. 7: Asymptotic decay of the depletion potential between a single big colloidal particle and a semipermeable planar membrane. Shown are the results of the WB theory (solid lines) and the asymptotic forms evaluated from Eqs. (23)-(24) (dashed lines). $\sigma_C = 3\sigma_A$ and the packing fractions are $\eta_A = 0.05$ and $\eta_B = 0.35$ for the potential marked as (a), $\eta_A = 0.1435$ and $\eta_B = 0.2565$ for the potential marked as (b), and $\eta_A = 0.35$ and $\eta_B = 0.05$ for the potential marked as (c). Potentials (b) and (c) are shifted by $\ln|\beta W(z)| = 10$ and 20, respectively.

functions $c_{ij}(r)$ and their Fourier transforms are readily obtained from the density functional theory

$$\begin{aligned} c_{ij}(r) &= -\beta \frac{\delta^2 F_{ex}[\rho_A(\mathbf{r}), \rho_B(\mathbf{r})]}{\delta \rho_i(\mathbf{r}) \delta \rho_j(\mathbf{r}')} \\ &= -\sum_{\alpha, \beta} \frac{\partial^2 \Phi(\{n_\nu\})}{\partial n_\alpha \partial n_\beta} w_\alpha^{(i)} \otimes w_\beta^{(j)}. \end{aligned} \quad (23)$$

In the above \otimes denotes the convolution. Explicit expressions for $c_{ij}(r)$ can be found in Ref.⁵⁴.

The asymptotic decay for pair correlations determines the decay of other structural and thermodynamic quantities describing inhomogeneous fluids. Thus the asymptotics of the depletion potential between a hard-sphere colloidal particle and a semipermeable planar membrane, for systems away from a crossover point, can be written as

$$\beta W(z) \sim A_d \exp(-a_0 z) \cos(a_1 z - \Theta_d). \quad (24)$$

The amplitude A_d and the phase Θ_d of the depletion potential depend on the external potential whereas the characteristic decay length a_0^{-1} and the oscillation wavelength $2\pi/a_1$ are the same as in the decay of the pair correlation functions. However in the proximity of a crossover point a two-pole approximation is necessary

$$\beta W(z) \sim A_d \exp(-a_0 z) \cos(a_1 z - \Theta_d)$$

$$+ \tilde{A}_d \exp(-\tilde{a}_0 z) \cos(\tilde{a}_1 z - \tilde{\Theta}_d). \quad (25)$$

In Fig. 7 we show the depletion potentials between a single big hard sphere of diameter $\sigma_C = 3\sigma_A$ and a semipermeable planar membrane. All potentials were evaluated for the constant total packing fraction of the smaller spheres, $\eta_A + \eta_B = 0.4$. The potential marked by (a) is for $\eta_A = 0.05$ and $\eta_B = 0.35$, whereas the potential marked by (c) is for $\eta_A = 0.35$ and $\eta_B = 0.05$. We find that for the system (a), rich in B species, the real part of the leading order pole $a_1 = 3.28257\sigma_A^{-1}$. This leads to the oscillation wavelength $1.91411\sigma_A$, which is close to σ_B . On the other hand, for the system (c), rich in A species, $a_1 = 6.41187\sigma_A^{-1}$ and this leads to the oscillation wavelength $0.97993\sigma_A$. The asymptotic form [cf. Eq. (24), dashed lines in Fig. 7] agrees very well with the DFT results (solid lines) already for separations of the order of several diameters. The depletion potential (b) was calculated for $\eta_A = 0.1435$ and $\eta_B = 0.2565$. These packing fractions are very close to the crossover point. We note that the asymptotic form, Eq. (25), gives an excellent approximation already for $z > 5\sigma_A$. This is the consequence of the fact that the asymptotic form sets in at intermediate separations. We conclude that the asymptotics of the depletion potential near a semipermeable membrane is the same as for the potential of the same mixture near a nonpermeable wall.

V. CONCLUSIONS

Within the framework of density functional theory we have investigated the effect of the membrane permeability on depletion potentials in colloidal systems. We have focused on highly idealized systems and considered hard sphere colloids and an infinitely thin ideal membrane. The main conclusion is that the colloid-semipermeable membrane effective interactions are generally weaker than those near a hard nonpermeable wall. For hard-sphere-ideal-membrane systems this finding can be ascertained by analyzing statistical-mechanical sum rules which relate the osmotic pressure to the contact value of the density profile of the nonpermeable component. We have found that the depletion potential gets stronger with an increase of the packing fraction of the nonpermeable species and with the osmotic pressure. The structure of the depletion potential and its asymptotics is the same as for the hard wall systems. In particular, we have found the structural crossover behavior that separates two distinct asymptotic regimes of the depletion potential. Likewise, the influence of the membrane curvature on the effective potential is similar to the hard-wall case but the effect is moderated. Although no comparison with computer simulation is presented we expect our White-Bear theory results to be very accurate.

It follows from the present study that in order to induce sufficiently strong colloid-membrane attraction the membrane should have high enough curvature. This effect can be brought about by changing locally the shape

of the membrane in the near vicinity of a colloidal particle and our results underline the importance of this process. Another possibility is to increase the osmotic pressure.

Acknowledgments

This work has been supported by KBN of Poland under the Grant 3T09A 069 27 (years 2004-2006).

-
- * Electronic address: pawel@paco.umcs.lublin.pl
- ¹ Likos, C. N. *Phys. Rep.* **2001**, *348*, 267.
 - ² Poon, W. C. K. *J. Phys.: Condens. Matter* **2002**, *14*, R859.
 - ³ Tuinier, R.; Rieger, J.; de Kruijff, C. G. *Adv. Colloid Interface Sci.* **2003**, *103*, 1.
 - ⁴ Dickman R.; Attard P.; Simonian V. *J. Chem. Phys.* **1997**, *107*, 205.
 - ⁵ Biben T.; Bladon P.; Frenkel D. *J. Phys.: Condens. Matter* **1996**, *8*, 10799.
 - ⁶ Asakura, S.; Oosawa, F. *J. Chem. Phys.* **1954**, *22*, 1255.
 - ⁷ Vrij, A. *Pure Appl. Chem.* **1976**, *48*, 471.
 - ⁸ Attard, P. *J. Chem. Phys.* **1990**, *92*, 4970.
 - ⁹ Attard, P.; Parker J. L. *J. Phys. Chem.* **1992**, *96*, 5086.
 - ¹⁰ Amokrane, S. *J. Chem. Phys.* **1998**, *108*, 7459.
 - ¹¹ Kinoshita, M.; Oguni, T. *J. Chem. Phys.* **2002**, *116*, 3493.
 - ¹² Götzelmann, B.; Evans, R.; Dietrich, S. *Phys. Rev. E* **1998**, *57*, 6785.
 - ¹³ Götzelmann, B.; Roth, R.; Dietrich, S.; Dijkstra, M.; Evans, R. *Europhys. Lett.* **1999**, *47*, 398.
 - ¹⁴ Roth, R.; Evans, R.; Dietrich, S. *Phys. Rev. E* **2000**, *62*, 5360.
 - ¹⁵ Bechinger, C.; Rudhardt, D.; Leiderer, P.; Roth, R.; Dietrich, S. *Phys. Rev. Lett.* **1999**, *83*, 3960.
 - ¹⁶ Helden, L.; Roth, R.; Koenderink, G. H.; Leiderer, P.; Bechinger, C. *Phys. Rev. Lett.* **2003**, *90*, 48301.
 - ¹⁷ Roth, R. *J. Phys.: Condens. Matter* **2003**, *15*, S277.
 - ¹⁸ Crocker, J. C.; Matteo, J. A.; Dinsmore, A. D.; Yodh, A. G. *Phys. Rev. Lett.* **1999**, *82*, 4352.
 - ¹⁹ Rudhardt, D.; Bechinger, C.; Leiderer, P. *Phys. Rev. Lett.* **1998**, *81*, 1330.
 - ²⁰ Dinsmore, A. D.; Yodh, A. G.; Pine, D. J.; *Nature* **1996**, *383* 239.
 - ²¹ Dinsmore, A. D.; Wong, D. T.; Nelson, P.; Yodh, A. G. *Phys. Rev. Lett.* **1998**, *80*, 409.
 - ²² Roth, R.; Götzelmann, B.; Dietrich, S. *Phys. Rev. Lett.* **1999**, *83*, 448.
 - ²³ König, P.-M.; Roth, R.; Mecke, K. R. *Phys. Rev. Lett.* **2004**, *93*, 160601.
 - ²⁴ König, P.-M.; Bryk, P.; Mecke, K. R.; Roth, R. *Europhys. Lett.* **2005**, *69*, 832.
 - ²⁵ Bickel, T. *J. Chem. Phys.* **2003**, *118*, 8960.
 - ²⁶ Murad, S.; Powles, J. G. In *Computational Methods in Colloid and Surface Science*; Borówko, M., Ed.; Marcel Dekker: New York, 2000; p 775.
 - ²⁷ Zhou, Y.; Stell, G. *J. Chem. Phys.* **1988**, *89*, 7010.
 - ²⁸ Zhou, Y.; Stell, G. *J. Chem. Phys.* **1988**, *89*, 7020.
 - ²⁹ Bryk, P.; Henderson, D.; Sokołowski, S. *J. Chem. Phys.* **1997**, *107*, 3333.
 - ³⁰ Bryk, P.; W. Cyrankiewicz; Borówko, M.; Sokołowski, S. *Mol. Phys.* **1998**, *93*, 111.
 - ³¹ Marsh, P.; Rickayzen, G.; Calleja, M. *Mol. Phys.* **1995**, *84*, 799.
 - ³² Margaritis, N.; Rickayzen, G. *Mol. Phys.* **1997**, *90*, 189.
 - ³³ Bryk, P.; Patrykiewicz, A.; Reszko-Zygmunt, J.; Sokołowski, S. *Mol. Phys.* **1999**, *96*, 1509.
 - ³⁴ Murad, S.; Madhusudan, R.; Powles, J. G. *Mol. Phys.* **1997**, *90*, 671.
 - ³⁵ Murad, S.; Oder, K.; Lin, J. *Mol. Phys.* **1998**, *95*, 401.
 - ³⁶ Borówko, M.; Bryk, P.; Pizio, O.; Sokołowski, S. *Mol. Phys.* **1998**, *94*, 867.
 - ³⁷ Jia, W.; Murad, S. *J. Chem. Phys.* **2005**, *122*, 234708.
 - ³⁸ Bryk, P.; Pizio, O.; Sokołowski, S. *Mol. Phys.* **1998**, *94*, 867.
 - ³⁹ Henderson, J.R. *Mol. Phys.* **1983**, *50*, 741.
 - ⁴⁰ Henderson, J. R. In *Fluid Interfacial Phenomena*; Croxton, C. A., Ed.; Wiley: Chichester, 1986; p 555.
 - ⁴¹ Samborski, A.; Stecki, J.; Poniewierski, A. *J. Chem. Phys.* **1993**, *98*, 8958.
 - ⁴² Martina, E. *Chem. Phys. Lett.* **1983**, *94*, 205.
 - ⁴³ Powles, J. G.; Holtz, B.; Evans, W. A. B.; Murad, S. *Mol. Phys.* **1997**, *90*, 665.
 - ⁴⁴ Jimenez-Angeles, F.; Lozada-Cassou, M. *J. Phys. Chem. B* **2004**, *108*, 1719.
 - ⁴⁵ Bryk, P.; Roth, R.; Mecke, K.R.; Dietrich, S. *Phys. Rev. E* **2003**, *68*, 031602.
 - ⁴⁶ Evans R. *Adv. Phys.* **1979**, *28*, 143.
 - ⁴⁷ Rosenfeld, Y. *Phys. Rev. Lett.* **1989**, *63*, 980.
 - ⁴⁸ Rosenfeld, Y. *J. Chem. Phys.* **1993**, *98*, 8126.
 - ⁴⁹ Roth, R.; Evans, R.; Lang, A.; Kahl, G. *J. Phys.: Condens. Matter* **2002**, *14*, 12063.
 - ⁵⁰ Yu, Y.-X.; Wu, J. *J. Chem. Phys.* **2002**, *117*, 10165.
 - ⁵¹ Bryk, P.; Roth, R.; Schoen, M.; Dietrich, S. *Europhys. Lett.* **2003**, *63*, 233.
 - ⁵² Evans, R.; Henderson, J. R.; Hoyle, D. C.; Parry, A. O.; Sabeur, Z. A. *Mol. Phys.* **1993**, *80*, 755.
 - ⁵³ Evans, R.; Leote de Carvalho, R. J. F.; Henderson, J. R.; Hoyle, D. C. *J. Chem. Phys.* **1994**, *100*, 591.
 - ⁵⁴ Grodon, C.; Dijkstra, M.; Evans, R.; Roth, R.; *J. Chem. Phys.* **2004**, *121*, 7869.
 - ⁵⁵ Grodon, C.; Dijkstra, M.; Evans, R.; Roth, R.; *Mol. Phys.* **2005**, *103*, 3009.